

Towards Efficient Automated Characterization of Irregular Histology Images via Transformation to Frieze-Like Patterns

Brian A. Canada¹, Georgia K. Thomas⁴, Keith C. Cheng^{1,4}, James Z. Wang^{1,2,3}, Yanxi Liu³

¹Integrative Biosciences Program, ²College of Information Sciences and Technology,
and ³College of Engineering, The Pennsylvania State University, University Park, PA, USA

⁴Penn State College of Medicine, Hershey, PA, USA
{canada, gkt104, kcheng, jwang, yul11}@psu.edu

ABSTRACT

Histology is used in both clinical and research contexts as a highly sensitive method for detecting morphological abnormalities in organ tissues. Although modern scanning equipment has enabled high-throughput digitization of high-resolution histology slides, the manual scoring and annotation of these images is a tedious, subjective, and sometimes error-prone process. A number of methods have been proposed for the automated characterization of histology images, most of which rely on the extraction of texture features used for classifier training. The irregular, nonlinear shapes of certain types of tissues can obscure the implicit symmetries observed within them, making it difficult or cumbersome for automated methods to extract texture features quickly and reliably. Using larval zebrafish eye and gut tissues as a pilot model, we present a prototype method for transforming the appearance of these irregularly-shaped tissues into one-dimensional, “frieze-like” patterns. We show that the reduced dimensionality of the patterns may allow them to be characterized with greater efficiency and accuracy than by previous methods of image analysis, which in turn enables potentially greater accuracy in the retrieval of histology images exhibiting abnormalities of interest to pathologists and researchers.

Categories and Subject Descriptors

J.3 [Life and Medical Sciences]: *Biology and genetics, health, medical information systems*; H.3.1 [Information Storage and Retrieval]: *Content Analysis and Indexing – Abstracting methods, indexing methods*; I.5.2 [Pattern Recognition]: *Design Methodology – Feature evaluation and selection, pattern analysis*.

General Terms

Algorithms, Experimentation, Performance

Keywords

Automated Histology, Computational Symmetry, Dimension Reduction, Frieze Patterns, Texture Analysis, Zebrafish



Figure 1. An example image of a histological section of a zebrafish larva.

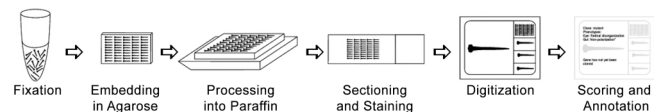


Figure 2. Current laboratory pipeline for “high-throughput” histology. The overall process is rate-limited by the manual (and tedious) process of scoring and annotation.

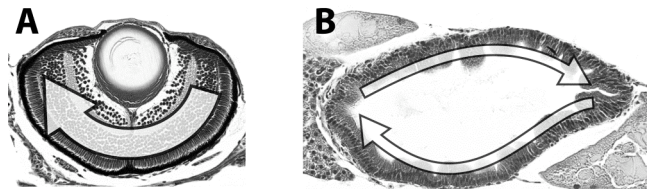


Figure 3. There is an implicit “rotational symmetry” in certain histology images, such as those of the zebrafish eye (a) and gut (b), as indicated by the arrows. Our challenge here is to recover and characterize this implicit symmetry.

1. INTRODUCTION

1.1 The need for automated characterization and retrieval of histological images

The study of systems biology involves the computational modeling and analysis of complex biological systems [1]. Whether the system of interest is a cell, an organ system, or a complete organism, a working model requires a comprehensive understanding of the functions of genes, interactions between gene products, and interactions between the system and its surrounding environment, all within the context of a particular biological process. A proper characterization of the process dynamics requires an integrated, spatiotemporal assessment of the abnormal phenotypes (observable traits) that result from the disruption of normal gene function due to mutations, knockdowns and knockouts, as well as toxicological or environmental effects.

Since many genes function across multiple tissue types, it is not surprising that many of these phenotypes cross organ systems to qualify as pleiotropy—the association of multiple phenotypes

Permission to make digital or hard copies of all or part of this work for personal or classroom use is granted without fee provided that copies are not made or distributed for profit or commercial advantage and that copies bear this notice and the full citation on the first page. To copy otherwise, or republish, to post on servers or to redistribute to lists, requires prior specific permission and/or a fee.

CIVR'08, July 7–9, 2008, Niagara Falls, Ontario, Canada.

Copyright 2008 ACM 978-1-60558-070-8/08/07...\$5.00.

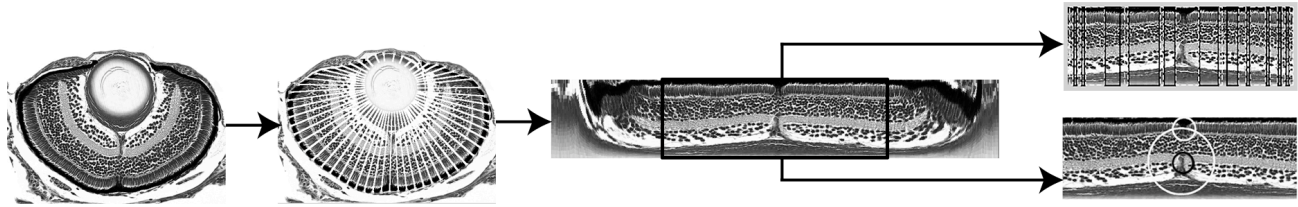


Figure 4. Example results of proposed methods. The implicitly symmetric region of interest is extracted from the image and then transformed into a 1-D “frieze-like” expansion. For retinal images, the extreme ends of the frieze-like expansion will be distorted, so we extract the middle 50% of pixels. The frieze-like expansion is then divided into regions according to similarity to the dominant motif. In addition, we convolve the image with a log-Gabor filter to detect potential local defects.

with a single gene defect. The existence of pleiotropy motivates the need for tools powerful enough to simultaneously survey multiple phenotypes. Automatic characterization of histological abnormalities can be an effective, high-throughput means of providing that important function.

Histology—the microscopic study of tissues—is a highly sensitive method of detecting and characterizing morphological phenotypes. Traditionally, histology is used in pathology for diagnosis of diseases such as cancer, although it has more recently become a powerful tool for studying functional genomics in the laboratory. Histology is particularly well suited to small model organisms, because all tissues in the organism can be sampled in a relatively small number of slides. Larval zebrafish, for example, are small enough to make it practical to assess tissue abnormalities in stained tissue sections from multiple specimens on single microscope slides. These “arrays” of larval tissue sections have been used to screen for abnormalities and can be readily digitized using modern scanning equipment and stored as high-resolution “virtual slides” for subsequent scoring and annotation of phenotypes.

A number of obstacles prevent histological analysis from reaching its maximum potential as a phenotyping tool, however. While largely reliable and useful clinically, the qualitative aspects of current histological assessments result in intra- and inter-observer variability owing to differences in training, ability, timing, and experience [2,3]. Moreover, because most histological images are characterized manually, a biologist must sift through dozens or even hundreds of images to find those images of specimens that exhibit any mutant phenotypes or otherwise abnormal traits. A mechanism to retrieve only those images with abnormal features would greatly enhance the productivity of biologists who take advantage of histology as a phenotyping tool.

1.2 Use of the zebrafish for high-throughput histological phenotyping studies

The zebrafish is an excellent model organism for vertebrate development and human disease because its transparent, readily accessible embryo develops outside the mother’s body [4]. Moreover, the zebrafish embryo develops much more rapidly than many other vertebrate models, with most organ systems well differentiated within 7 dpf (days post-fertilization) [5], allowing mutant phenotypes to be identified quickly. Owing to their small size, zebrafish larvae are amenable to “high-throughput” histology, a procedure developed by Cheng and co-workers [6, 7, 8, 9] in which arrays of up to 50 zebrafish larvae at different stages of development are fixed to preserve morphology,

embedded in agarose gel, processed into paraffin wax blocks, and sliced into thin sections. The sections are individually mounted on glass microscope slides for staining and then scanned to produce virtual slides for scoring and annotation of phenotypes (Fig. 2).

The phrase “high-throughput,” as used in this context, does not currently apply to all steps in the cycle, however. While fixation, embedding, sectioning, staining, and digitization of an entire array of larvae may be conducted in parallel (in that multiple larvae are processed simultaneously), the process of scoring each image is rate limiting. Our early efforts to address this problem resulted in a prototype method for the automated segmentation and classification of histological images of larval zebrafish eye and gut [10]. In this prototype, called SHIRAZ (System of Histological Image Retrieval and Annotation for Zoopathology), the segmentation and feature extraction algorithms as well as classification models were initially designed to analyze images of larval zebrafish eye and gut as part of our lab’s ongoing study of pleiotropic genes in the zebrafish.

We chose eye and gut as the initial organs for examination because their tissues have an inherent polarity and “directional” organization that, when disrupted, result in mutant phenotypes that are relatively easy to detect and have also been shown to co-segregate across organ boundaries as a result of pleiotropy in our mutant screen [11]. Our prototype yielded highly promising initial results for both segmentation and classification, and to our knowledge, this was the first published work in automated zebrafish histology image analysis. However, classification was limited to assigning a categorical abnormality score to each image and did not specifically focus on the detection of local tissue defects in mutant specimens. This was mainly due to segmentation difficulties arising from the irregular shapes of the cell layers as well as very subtle variations in gray-level intensity and texture between certain layers.

Upon inspection of any typical zebrafish histology image, one can observe that certain tissue structures exhibit a certain degree of repetition or symmetry (at least in the normal or “wild-type” state). One can see that the zebrafish larval retina possesses partial rotational symmetry about the lens, as indicated in Fig. 3a. In addition, despite its distorted and folded appearance, the epithelial lining of the zebrafish gut seems to resemble a repeating pattern of columnar cells (see Fig. 3b), each of which normally has a polarized orientation, with the nucleus on one end of the column and the cytoplasm on the other. The repeating patterns implied within the retina and the gut epithelium might become more obvious if one could somehow transform the image of the gut from its folded appearance to a more regular, linear shape, thereby reducing the pattern complexity to only one dimension. This

would facilitate the generation of methods for detecting and characterizing the implicit symmetry patterns as well as defects and local deviations that disrupt the pattern continuity.

We have explored the development of such transformation and detection methods [12], and we here present a novel approach to the detection and characterization of tissue defects in these types of histology images. Specifically, we make three contributions:

- (1) We propose a method to segment out the regions of interest within certain types of histological structures—here using zebrafish eye and gut as a pilot model—and transform these regions to a one-dimensional pattern;
- (2) We propose a method to detect the dominant or most commonly repeated motif within each pattern and then use the differences in global texture (measured using Haralick and Gabor features) between the dominant motif and the remainder of the pattern as a set of features to classify the images as normal or abnormal; and
- (3) We demonstrate that transformation of these images to a 1-D pattern greatly simplifies the reliable detection of potential local texture defects using log-Gabor filters.

The information extracted from these methods will be used as part of an ontology-based zebrafish histology image annotation and retrieval system currently under development. Fig. 4 provides a result from the transformation and characterization of an example input image.

2. RELATED WORK

2.1 Symmetry detection

Recently, Lee *et al.* [13] proposed a new algorithm for rotational symmetry detection and characterization using a “frieze-expansion” approach, in which 2-D images consisting of potential centers of rotational symmetry are transformed from polar to rectangular coordinates with respect to each potential symmetry center, thereby producing a *frieze pattern*. A frieze pattern is any pattern that exhibits 1-D translational symmetry. Group theory [14] has proven that there are only seven unique frieze symmetry groups (shown in Fig. 5), with each of these seven groups corresponding to a type of *rotational* symmetry group, such as cyclic (C_n) or dihedral (D_n), where n represents the number of discrete rotational symmetries exhibited in the pattern. Since frieze patterns are symmetric in only one direction, the task of detecting the repeated pattern motif becomes considerably easier. Following the frieze-expansion step, the symmetry group is

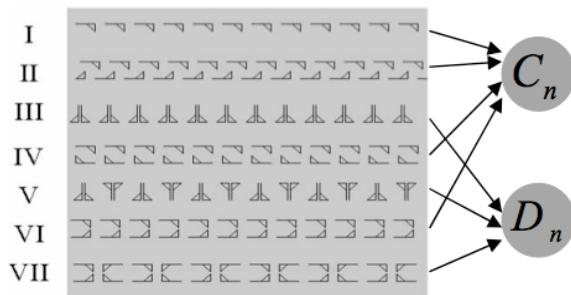


Figure 5. The correspondence between the seven frieze groups and the two discrete rotation symmetry groups in 2-D. From Lee *et al.* [13]; used with permission.

determined by frequency analysis using Discrete Fourier Transform (DFT). This approach to rotational symmetry detection was found to be superior in terms of accuracy and speed to current state-of-the-art rotational symmetry detection algorithms, including the SIFT keypoint-based method proposed by Loy and Eklundh [15] and the gradient vector flow (GVF) approach proposed by Prasad and Davis [16]. In this paper, we propose a variation of Lee’s frieze-expansion approach in the analysis of certain types of histopathology images that appear to possess an implicit “rotational” symmetry.

2.2 Texture analysis in histopathology images

A common approach to analyzing texture in histological and other images is based on features computed from an image’s gray-level co-occurrence matrix (GLCM). Each element in the GLCM represents the probability $p(i, j)$ of a pixel with gray-level intensity i having a neighboring pixel with gray-level intensity j . Because features computed from the GLCM consider the values of two neighboring pixels, they are termed *second-order* texture features, in contrast to *first-order* measures of textures such as mean and standard deviation, which do not specifically account for relationships between pixels.

Haralick [17] introduced a number of commonly used second-order texture features, including *energy* (also known as the *angular second moment* or *uniformity*), *entropy*, *heterogeneity* (also known as the *inverse difference moment*), *contrast* (also called *variance* or *inertia*), as well as several additional measures of variance, entropy, and correlation. Closely related to entropy (but not considered a “Haralick feature”) is *mutual information*, which is the difference between the joint entropy of two images taken together and the sum of each image’s marginal entropy. Maximization of mutual information has been used as a criterion for alignment of two similar images [18], but here we will simply use mutual information as one possible measure of image similarity.

In addition to the Haralick features derived from an image’s GLCM, features resulting from images convolved with Gabor filters have been used to detect responses to global textural variation. Part of the usefulness of Gabor filters stems from their ability to approximate certain characteristics of how information is processed in the primary visual cortex [19]. In addition, they have been shown to possess optimal localization properties in both spatial and frequency domains. Consequently, they are a good choice for the segmentation and characterization of image textures.

In one recent application, Doyle *et al.* [20] used both Haralick and Gabor features in the classification of prostate cancer histology images, with scoring based on the Gleason grading system commonly used in prostate cancer diagnosis. Using a support vector classifier, Doyle *et al.* were able to successfully discriminate between images of varying Gleason score, ranging from 1 (normal or benign, with gland boundaries readily identified) to 5 (severely abnormal, with no recognizable glands), with accuracies ranging from 77% to 93% depending on the choice of classification pairs used.

It was suggested by Field in 1987 [21], however, that Gabor functions tend to over-represent low frequency components and under-represent higher-frequency components and thus may not always be suitable for texture analysis of natural images. Field proposed an alternative, called the *log-Gabor* function, whose

transfer function is Gaussian when viewed on logarithmic frequency scales. Its frequency response is represented in linear frequency space by the equation

$$G(f) = \exp \left(-\frac{1}{2} \cdot \frac{\left(\log \frac{f}{f_0} \right)^2}{\left(\log \frac{\sigma}{f_0} \right)^2} \right)$$

where f_0 is the center frequency of the filter and σ is the standard deviation of the Gaussian that describes the behavior of the log-Gabor filter's transfer function in the frequency domain. The ratio σ / f_0 is thus used in specifying the filter bandwidth. Because its frequency response is more symmetric on the logarithmic scale, the log-Gabor function may be more consistent with measurements of cell responses in mammalian visual systems, which are also symmetric on the log frequency scale [22]. Like Gabor functions, however, log-Gabor functions are typically implemented using banks of filters generated using multiple scales and orientations.

In our work, we not only classify images of zebrafish eye and gut histology using both Haralick and log-Gabor features, but we also show that log-Gabor filters applied in only one direction may be useful for detecting possible local tissue defects in our frieze-like image transformations.

3. PROPOSED METHODS

Unlike the algorithm by Lee *et al.* [13], which is designed to detect and characterize patterns exhibiting true rotational symmetry, our method had to be designed to extract and process patterns too irregular to have explicit rotational symmetry. In other words, the variation in cell shape, color, and texture along the gut epithelium or the retinal cell layers makes it unlikely that the entire image can be represented by one single motif, *i.e.*, a local tile reflecting the symmetry of the entire pattern. Consequently, the “hard” classifications produced by Lee’s algorithm, *e.g.*, “ C_5 ” for a cyclic pattern with five rotational symmetries, are less useful for our purposes.

Upon inspection of most eye and gut images, however, there may be a *dominant* motif—that is, a motif that is observed in the pattern more often than other motifs. In other words, given an image divided into tiles (or *texels*) of identical size, if a *plurality* of texels are highly similar, then any of the texels in that plurality could be considered the dominant motif, although we would naturally expect at least *some* variability among these texels. The remaining texels in the pattern would then be grouped and characterized according to their extent of dissimilarity from the dominant motif. Texture features are then extracted from each group of texels and later used for classifying the entire pattern, *e.g.*, as either normal (“wild-type”) or abnormal (“mutant”). Therefore, the proposed framework for pattern characterization can be summarized in the following steps:

- (1) *Extraction* of the implicitly repeating pattern from the image followed by *transformation* into its 1-D “frieze-like expansion”
- (2) *Classification* of the pattern as normal or abnormal, based on texture features extracted from texels grouped by extent of similarity to the recovered dominant motif

- (3) *Detection of local texture defects* within the frieze-like expansion pattern using log-Gabor filters applied in the direction of 1-D pattern repetition.

The extracted features and the global classification of the pattern, as well as the locations of potential defects therein, may be used to index and annotate the original images for later retrieval, such as for searching for images of similar phenotype using a previously uncharacterized image as the search query.

3.1 “Frieze-like” expansion

3.1.1 Image pre-processing and segmentation

Zebrafish larvae were collected, fixed, and embedded as described in [6,7]. Eye and gut images were manually cropped from 40× virtual slides of hematoxylin & eosin (H&E)-stained zebrafish sections captured using an Aperio ScanScope™ slide scanner in the Penn State Zebrafish Functional Genomics Facility. In order to reduce the computational cost of image segmentation and feature extraction, the images of the zebrafish eyes and guts used in our prototype were converted to grayscale color space and finally scaled down to a 512×512 matrix.

Segmentation of the zebrafish larval eye and gut images is carried out by a series of image processing operations including histogram equalization, connected component analysis, thresholding, edge detection, as well as the morphological operations of dilation, erosion, closing, and opening. The parameters used for each of these operations were heuristically determined, but are a loose function of the skewness of the image histogram.

The zebrafish eye consists of several distinct layers, including the lens, the ganglion cell layer (GCL), the inner plexiform layer (IPL), the inner nuclear layer (INL), the outer plexiform layer (OPL), the photoreceptor layer (PRL), and the retinal pigmented epithelium (RPE) [5]. For the purposes of expanding the retina into a 1-D frieze-like pattern, we only need to provide an outer perimeter, which will correspond the top edge of the frieze-like expansion pattern, and an inner perimeter, corresponding to the bottom edge (Figs. 8b,c). Thus we need only extract the RPE and the lens, and fortunately, they are relatively easy to identify. The RPE, by virtue of its melanin pigmentation, is always the darkest

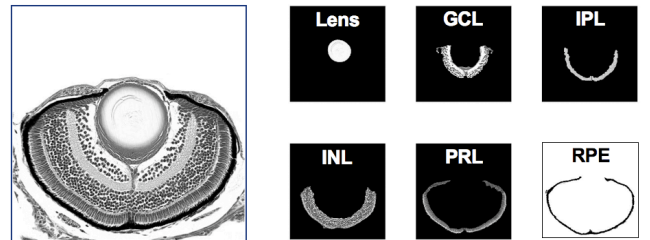


Figure 6. Example segmentation of a zebrafish eye (left) into its constituent cell layers.



Figure 7. Example segmentation of a zebrafish gut image (left) into the epithelial lining and the lumen.

continuous segment of the retina, and the lens is always the largest object whose shape most closely approximates that of a circle.

For gut images, the segmentation (Fig. 7) starts with the detection of the lumen (the “open” area within the gut), followed by an approximate segmentation of the epithelial lining, consisting of the columnar enterocyte cells. For the purposes of image transformation, we will use the exterior boundary of the epithelial lining (roughly corresponding to the basement membrane) as the outer perimeter, and the boundary of the lumen as the inner perimeter.

3.1.2 Image transformation

The perimeter points are used as a basis for extracting line segments of pixels from the original eye or gut histology image. Ideally, each line segment would start at the outer perimeter and be oriented more or less perpendicular to the tangent line at the starting point. The intersecting point on the inner perimeter would thus be the endpoint of the line segment. However, owing to the irregular shape of both perimeters, the line segment may not necessarily end at the desired point on the inner perimeter; in fact, in some cases the line perpendicular to the tangent line at the starting point may not even intersect with the inner perimeter at all. To remedy this, the algorithm identifies a set of initial *control points* evenly spaced around the outer perimeter (in practice, 12 control points usually provides good results). Line segments are extracted starting from these control points and ending at the *nearest* point on the inner perimeter as measured by Euclidean distance. The remaining line segments are then extracted by interpolation between the control points (Fig. 8c).

Following extraction of all line segments, we normalize their lengths to a pre-specified number of pixels. The normalized line segments are then rearranged as columns of the transformed image (Fig. 8d). Since the layers of the larval retina exhibit only partial rotational symmetry around the lens, the resulting image will be distorted at either end of the frieze expansion. In practice, the middle 50% of the transformed image is most highly representative of the retina’s partial rotational symmetry around the lens, so we perform our subsequent analysis only on this central range, and ignore the more highly distorted sections at either end of the original transformed image.

3.2 Pattern characterization

3.2.1 Recovery of dominant pattern motif

We begin by dividing the transformed image into a contiguous set of tiles (texels) of equal width (default = 10 pixels), as in Fig. 8e. We wish to determine which of these texels matches a plurality of the remaining texels. For each texel, proceeding from left to right across the image, we use correlation (performed in the frequency domain via discrete Fourier transform, or DFT) to score the degree to which the selected candidate texel matches each of the other texels in the image, as in Fig. 8f. More specifically, the score at each texel location is simply taken as the height of the central peak of the correlation image after normalization to a standard grayscale value range of zero to 255. Texels that score above a pre-chosen threshold (usually within 90 to 95% of the maximum) are identified as strong matches. The scores of the remaining texels are then used to identify them as either “marginal” or “weak” (Fig. 8g). We then compute the fractions of strong, marginal, and weak matches for each candidate texel. Once all such candidate texels have been evaluated, the *dominant motif* is the candidate texel which yields the largest fraction of

strong correlation matches among all texels in the image. Optionally, this step could be repeated using candidate texels of different widths, but given the inherent irregularity within the pattern, it is probably unrealistic to expect any repeating motifs in the pattern to have the same width. Rather, we only wish to achieve a rough “segmentation” of the pattern into texels that are grouped according to their degree of similarity to the dominant motif.

3.2.2 Feature extraction

We are interested in seeing which image features, if any, can be used to discriminate between normal (wild-type) or abnormal (mutant) histology images. Because the image consists of additional texel groups whose texture patterns may vary significantly from the dominant motif, we cannot simply average the texture features from the whole image. Consequently, we extract three sets of features—one set for the group containing the dominant motif, and one set each for those texels with “marginal” and “weak” correlation scores. Each of the three sets of features includes:

- Mean and standard deviation of four Haralick texture features (*energy*, *contrast*, *entropy*, and *homogeneity*)
- Mean and standard deviation of the *mutual information* calculated between the dominant motif and all other texels in the current group
- Mean and standard deviation of the matrices generated from convolution of all within-group texels with a bank of log-Gabor filters (using $\sigma / f_0 = 0.65$, corresponding to a bandwidth of roughly 1.5 octaves) applied at six orientations over four scales, for a total of 24 filter convolutions.

Thus, each of the three motif sets yields 58 features, for a total of 174 texture features. Convolution of the log-Gabor filters with each texel is performed in the frequency domain via fast Fourier transform (FFT) as described in [22].

3.2.3 Binary classification

For the purpose of comparing classification results with those of the original SHIRAZ prototype [10], we once again make use of the classification and regression trees or “CART” algorithm [23] to classify the eye and gut images as either normal (i.e., “wild-type”) or abnormal (i.e., “mutant”). The CART algorithm works by finding a hierarchy of features that yield the best discrimination among the desired set of classes. At the “root node” of the tree, which represents the full data set, the best degree of discrimination (or “best split”) is computed for all features. Once a best split has been chosen for the root node, the data is partitioned into two “child” or “leaf” nodes. This process is repeated until a pre-chosen stopping criterion is reached, such as when the data has been partitioned enough so that all leaf nodes contain, at most, a specified maximum number of samples. After the tree is constructed, it may be found that “pruning” the tree back to a smaller number of terminal nodes may improve the overall classification accuracy.

3.3 Detection of local texture defects

One of the driving forces behind transforming irregular histology images into 1-D frieze-like patterns is that subtle defects in the image texture may be located simply by applying a log-Gabor function in the horizontal orientation, enabling the automated “scanning” of the transformed image, from left to right.

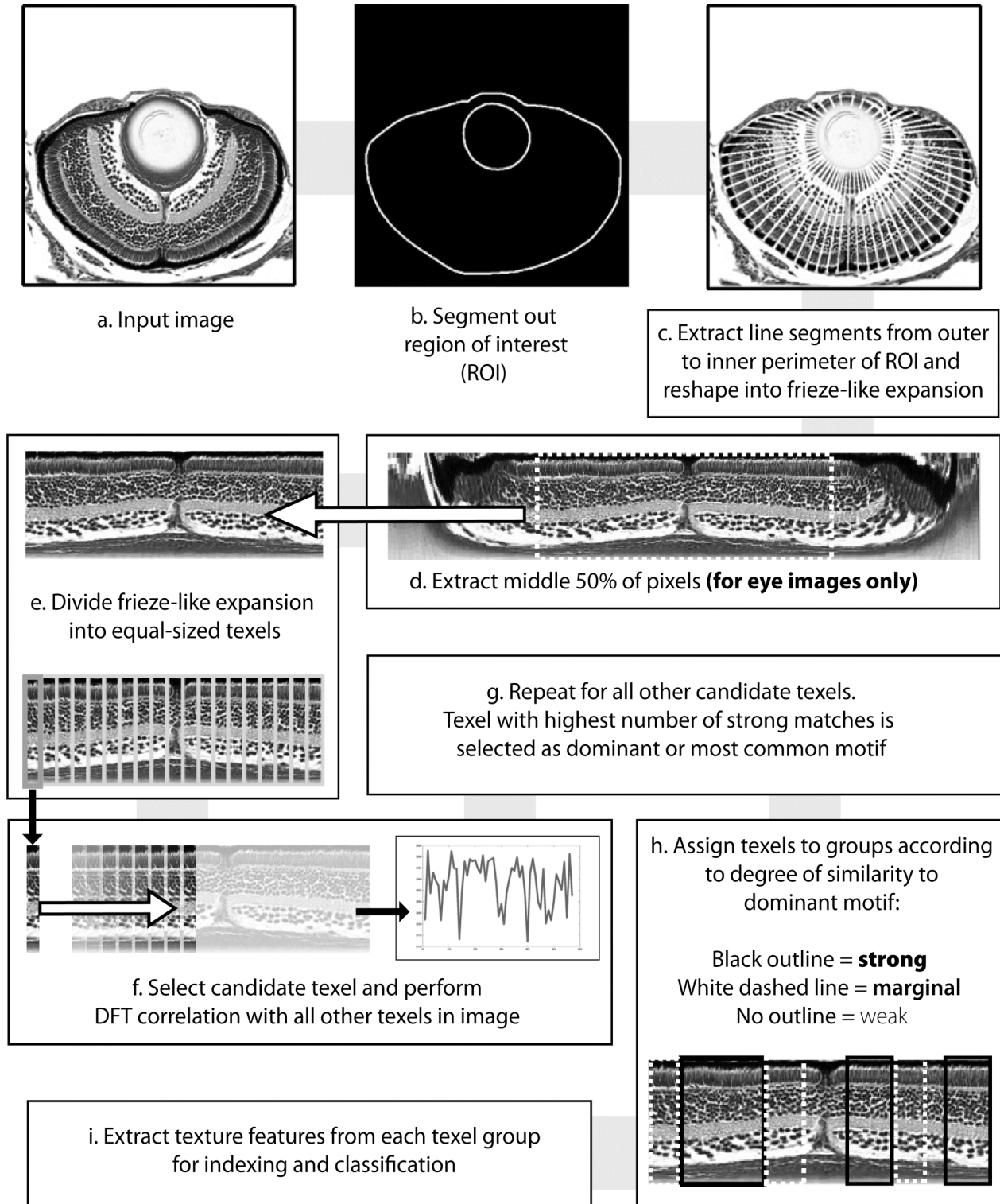


Figure 8. Illustration of algorithm for transformation of input image into frieze-like expansion, followed by recovery of dominant motif and extraction of features from texel groups. Please note that this figure is for illustrative purposes only and may not necessarily reflect the actual output from the algorithm.

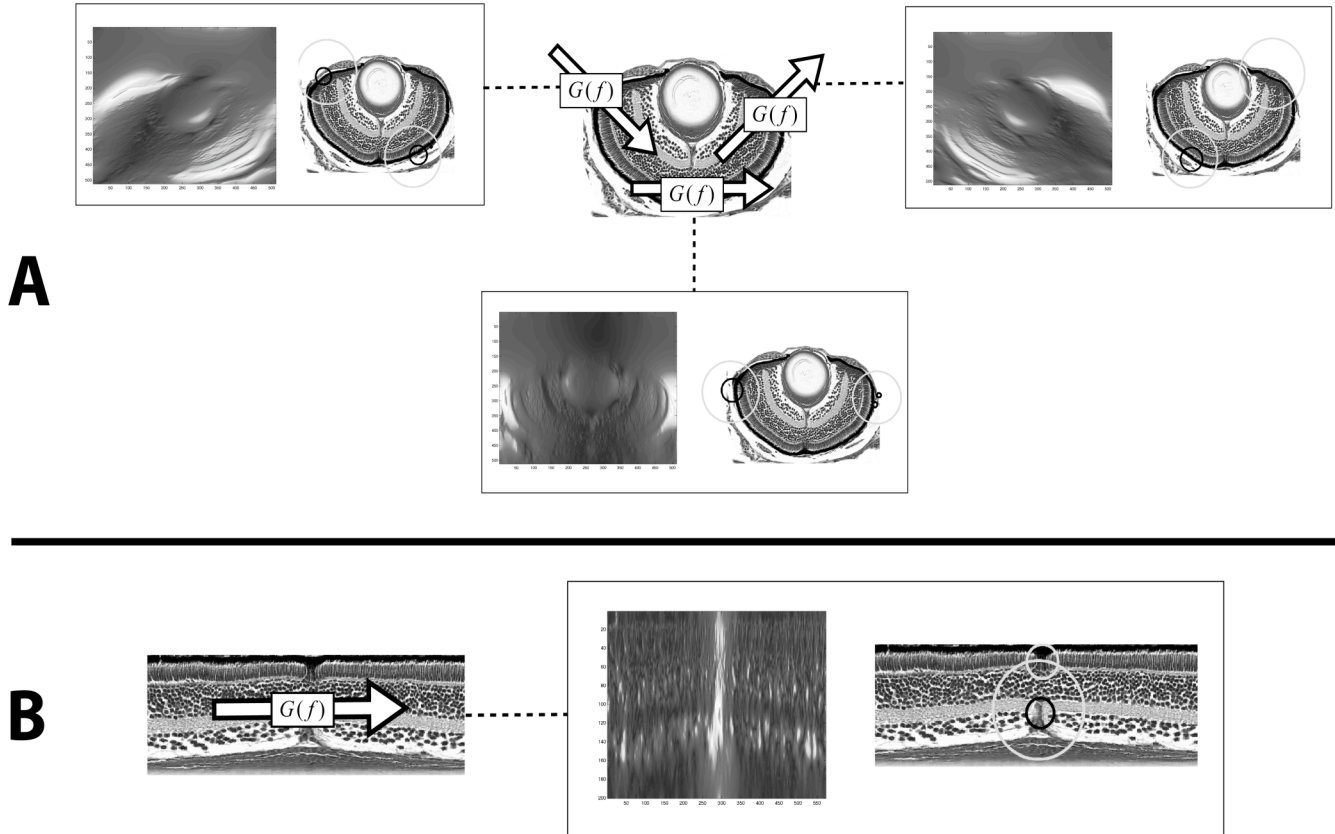


Figure 9. Illustration of the rationale behind using frieze-like expansions for texture defect identification by log-Gabor filter convolution. If we use the original, un-transformed image as in (a), we must convolve the log-Gabor filter $G(f)$ with the image using several filter orientations to account for the rotational symmetry of the retinal cell layers around the lens. In each of the three orientations shown (as indicated by the arrow directions), the log-Gabor filter mistakenly identifies the retinal pigmented epithelium (RPE) as the “defect” in the image. Only after extracting the retinal cell layers and transforming them into a one-dimensional frieze-like pattern as in (b) are we able to properly identify the texture “defect” of interest (which in this case is actually the optic nerve). The spectral output of each log-Gabor convolution is shown adjacent to its corresponding defect detection result. Lighter regions in the spectra correspond to higher peaks.

This is particularly useful for the frieze-expansion images of the retina, which has a generally ordered, laminar appearance, and so disruptions within a given layer can be readily localized by scanning horizontally.

While log-Gabor filters could be applied to the *original* retina image (prior to transformation) to scan for defects, two problems would arise, as illustrated in Fig. 9a. First, because of the rotational symmetry of the retinal layers about the lens, log-Gabor filters would have to be generated using multiple orientations, since the filter cannot proceed through a curved path like the retinal layers do. At best, the filter can be applied in an orientation roughly tangent to the rotation path at a given point, but the filter would only be useful over a short distance before a second filter at another orientation would have to be applied. The fact that multiple orientations are used causes the second problem, in that while a given filter (at a particular orientation) could detect a potential defect within a given cell layer or region, that same filter would undoubtedly yield several false positive signal peaks in other areas of the image, because the filter itself does not

discriminate between intra-region and inter-region texture differences. Presumably, if such filters could be designed to operate in polar coordinates, this might not be as much of a problem, but our solution is to instead transform the image from “polar-like” coordinates to a pattern that more or less varies only in the horizontal dimension, allowing a single log-Gabor filter to operate over the entire image and minimizing the risk of detecting false positive texture defects. Indeed, perhaps the single greatest advantage of using the frieze-expansion image for texture feature extraction and defect detection is that the results are *invariant* to the orientation of the original image.

Here, we generated a filter bank using ten scales over six orientations (of which only the horizontal orientation was used), and while the detection results are sensitive to the choice of scale and other parameters used, we found that the fifth scale out of 10, with σ / f_0 reduced to 0.001, yielded adequate bandwidth for detecting most of the important defects, particularly in the eye images, and so our results are based on those parameters.

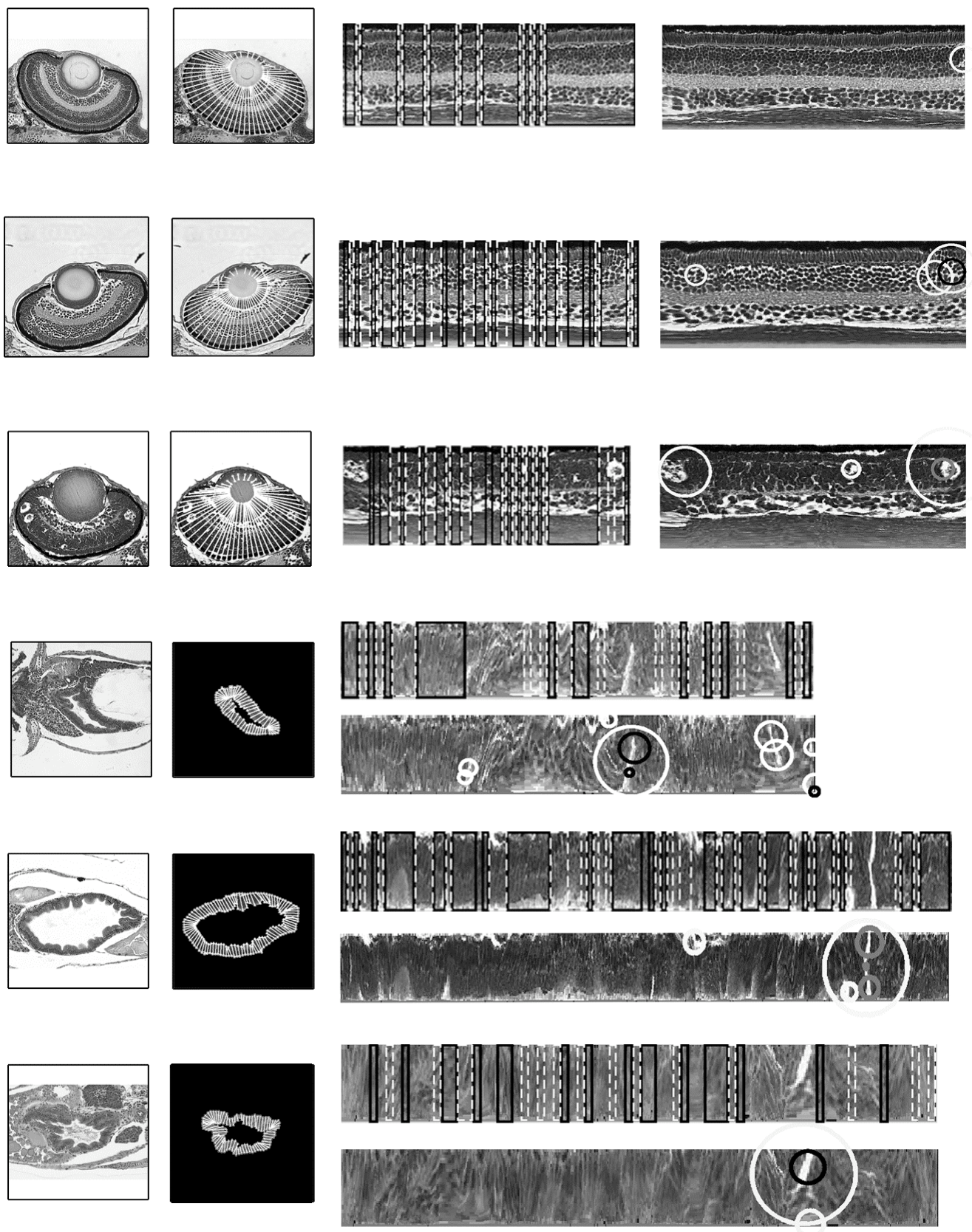


Figure 10. Example results of frieze expansion, texel grouping, and texture defect identification for selected eye and gut images.

4. RESULTS

4.1 Image expansion and classification

Fig. 10 shows selected examples of frieze-like expansions of the zebrafish eye and gut images, as well as the results of dividing each pattern into groups according to the extent of each texel’s similarity to the dominant motif.

For eye image classification, we used a set of 79 input images (38 wild-type, 41 mutant). Binary classification using the CART algorithm yielded 91% accuracy using both 10-fold cross validation as well as leave-one-out cross validation, with seven samples being misclassified. According to CART, the most discriminating feature was found to be the standard deviation of the log-Gabor filter convolution result, at scale 1 and orientation 4 (orientation angle = $\pi/2$).

Similarly, for gut image classification, we used a set of 78 input images (28 wild-type, 50 mutant). Binary classification using the CART algorithm yielded 92% accuracy using both 10-fold and leave-one-out cross validation, with only six samples being misclassified. In this case, the most discriminating feature was found to be the mean of the log-Gabor filter convolution result, at scale 4 and orientation 2 (orientation angle = $\pi/6$).

Table 1. Summary of binary image classification results

Organ	Proposed method (based on Frieze-like expansions)		Previous results (based on complete image segmentation, from [10])	
	10-fold CV	Leave- one-out CV	10-fold CV	Leave- one-out CV
Eyes	91%	91%	90%	87%
Guts	92%	92%	86%	86%

4.2 Image defect detection

Selected output results following texture defect detection for both eye and gut images are also shown in Fig. 10. The darker circles indicate the locations of peaks from the log-Gabor convolution output that rank in the 99.9th percentile (and are therefore considered “severe defects”), and the lighter circles correspond to peaks ranking in the 99th percentile (and are considered “potential defects”). For the purposes of making the defect detections easier to visualize, the size of the circle is equal to twice the equivalent diameter of the region surrounding each “cluster” of peaks. For the retinal images only, defects in the bottom third of each image are not shown due to the inherent variability of inter-nuclear spacing in the ganglion cell layer, which would otherwise result in several false-positive matches.

5. DISCUSSION

We believe that these results are quite promising in that they compare somewhat favorably to the binary classification accuracies we reported using the original SHIRAZ prototype [10], which used features extracted from images that had been completely segmented (see Table 1). The new results have the added advantage of being generated much more quickly, mainly because of the reduced reliance on image segmentation. While it previously required 3-4 minutes to completely segment and extract enough features from a typical retina image for

classification, we can now process the same image in less than one minute, with improved classification results.

The proposed methods do have some limitations. For example, the fidelity of the features extracted from the image is partially dependent on the quality of segmentation. Though fewer segmentation steps are used here, if the boundaries of the segmented regions are incorrect, parts of the resulting frieze-expansion image may have significant local distortions that can affect the extracted texture properties, though this appears to be less of a problem for the eye images than for the gut, since the basement membrane of the gut epithelium is sometimes difficult to detect by grayscale intensity differences alone. Moreover, the presence of multiple villi (finger-like projections into the lumen) can contribute to greater complexity of the undulating shape of the interior epithelial boundary, making the pairwise correspondence between outer and inner perimeter pixels less obvious for the gut than for the retina, which may also contribute to local distortions in the frieze-like pattern. We are currently exploring ways to overcome these issues.

Another limitation stems from the fact that we only use the middle 50% of pixels of the expanded retina images, due to there being only “partial” rotational symmetry around the lens. This means we are unable to use the proposed methods here to detect any defects in certain parts of the retina, such as the photoreceptor layer’s “marginal zones” located immediately adjacent to the lens.

Finally, we have tried to optimize the parameters of the log-Gabor filter kernel to be sensitive to subtle texture variations, particularly in the outer layers of the retina such as the photoreceptor layer, the inner nuclear layer, and the inner plexiform layer. Increasing that sensitivity does, however, amplify the detection of texture variation within the ganglion cell layer, which can result in a number of false positives due to variable spacing between ganglion cells occurring even in non-pathological images.

6. CONCLUSIONS AND FUTURE WORK

This is not intended to be a complete solution to the problem of automated histology image classification, which is a monumental task that years of research have yet to come close to solving. Rather, what we have hoped to convey is that transforming an image to what is essentially a “reduced-dimension” coordinate system may facilitate the detection of certain kinds of features. In our case, we are looking to find regions in an image where the naturally occurring (but implicit) symmetry is disrupted.

Ultimately, methods such as those proposed herein can be integrated into an image annotation and retrieval system for histopathologists or for researchers who use histology as a tool for mutant phenotyping. For example, the proposed methods might be used to rapidly screen a database of images of certain types of tissues and retrieve previously characterized images that exhibit specific defects of interest to the user, who may be trying to assign possible functions to a previously uncharacterized genetic mutation that results in morphological defects and pattern abnormalities similar to the retrieved images.

In terms of future work, an obvious next step might be to take advantage of the power of Gabor filters to recognize changes in texture at even higher magnification, enabling the detection of abnormalities between and within nuclei and other subcellular features. In another application best suited for the retina images,

we might consider applying vertically-oriented Gabor filters to the freeze-expanded retina image so that we can rapidly identify the boundaries between the various retinal layers (or even better, be able to distinguish between true layer boundaries and within-layer defects).

7. ACKNOWLEDGMENTS

Brian Canada (corresponding author) contributed the proposed methods and was responsible for the manuscript writing. He is with the Integrative Biosciences Graduate Program of the Huck Institutes of the Life Sciences and is supported by the Penn State Academic Computing Fellowship. Georgia Thomas and Keith Cheng, MD, PhD, who contributed the zebrafish images as well as invaluable suggestions to improve the relevance of the method to the biological community, are with the Department of Pathology. Prof. Cheng is supported by the National Institutes of Health (NIH) under Grant Nos. 5R24RR017441 and 5R01CA073935, as well as the Life Sciences Greenhouse of Central Pennsylvania and Pennsylvania Department of Health Tobacco Settlement Funds. James Z. Wang, PhD, is with the College of Information Sciences and Technology and specializes in novel applications in image annotation and retrieval. He is also affiliated with Carnegie Mellon University, Pittsburgh, PA, and his research has been supported by the National Science Foundation (NSF) under Grant Nos. 0347148 and 0202007. Yanxi Liu, PhD, is with the Department of Computer Science and Engineering and contributed the original “freeze-expansion” method as part of the Penn State course in Computational Symmetry, from which the current work was derived. She is also affiliated with Carnegie Mellon University as well as the University of Pittsburgh, and is supported by NSF, NIH, and the Pennsylvania Dept. of Health.

8. REFERENCES

- [1] Grabe, N., Pommerencke, T., Steinberg, T., Dickhaus, H., Tomakidi, P. (2007). “Reconstructing protein networks of epithelial differentiation from histological sections.” *Bioinformatics*. 23(23): 3200-3208.
- [2] Colquhoun, P., Nogueras, J.J., Dipasquale, B., Petras, R., Wexner, S.D., Woodhouse, S. (2003). “Interobserver and intraobserver bias exists in the interpretation of anal dysplasia.” *Dis Colon Rectum*. 46(10): 1332-1338.
- [3] Plummer, M., Buiatti, E., Lopez, G., Peraza, S., Vivas, J., Oliver, W., Munoz, N. (1997). “Histological diagnosis of precancerous lesions of the stomach: a reliability study.” *Int J Epidemiol*. 26(4): 716-720.
- [4] Bradbury, J. (2004). “Small fish, big science.” *PLoS Biology*. 2(5): E148.
- [5] Nusslein-Volhard, C., Dahm, R. (eds.) *Zebrafish: A Practical Approach*. Oxford: Oxford University Press; 2002.
- [6] Tsao-Wu, G.S., Weber, C.H., Budgeon, L.R., Cheng, K.C. (1998). “Agarose embedded tissue arrays for histologic and genetic analysis.” *Biotechniques*. 25(4): 614-618.
- [7] Sabaliauskas, N.A., Foutz, C.A., Mest, J.R., Budgeon, L.R., Sidor, A.T., Gershenson, J.A., Joshi, S.B., Cheng, K.C. (2006). “High-throughput zebrafish histology.” *Methods*. 39(3): 246-254.
- [8] Tsao-Wu, G.S., Weber, C.H., Budgeon, L.R., Cheng, K.C. (1999). “Agarose embedded tissue arrays for histologic and genetic analysis.” in *Expression Genetics: High-Throughput Methods*, Chapter 4, M. McClelland and A. Pardee (eds.). Natick, MA: Eaton Publishing; 1999.
- [9] Moore, J.L., Aros, M., Steudel, K.G., Cheng, K.C. (2002). “Fixation and decalcification of adult zebrafish for histological, immunocytochemical, and genotypic analysis.” *Biotechniques*. 32: 296-298.
- [10] Canada, B.A., Thomas, G.K., Cheng, K.C., Wang, J.Z. (2007). “Automated segmentation and classification of zebrafish histology images for high-throughput phenotyping.” *Proc. of the 3rd IEEE-NIH Life Science Systems and Applications Workshop*, pp. 245-248.
- [11] Mohideen, M.A., Beckwith, L.G., Tsao-Wu, G.S., Moore, J.L., Wong, A.C.C., Chinoy, M.R., Cheng, K.C. (2003). “Histology-based screen for zebrafish mutants with abnormal cell differentiation.” *Dev. Dynamics*. 228: 414-423.
- [12] Canada, B.A., Liu, Y. (2008). “Application of Computational Symmetry to Histology Images.” Penn State Dept. of Computer Science and Engineering Technical Report 08-001.
- [13] Lee, S., Collins, R.T., Liu, Y. (2008). “Rotation symmetry group detection via frequency analysis of freeze-expansions.” *Proc. of the 2008 IEEE Conference on Computer Vision and Pattern Recognition (CVPR 2008)*.
- [14] Grünbaum, B., Shephard, G.C. *Tilings and Patterns*. New York: W. H. Freeman and Company; 1987.
- [15] Loy, G., Eklundh, J. (2006). “Detecting symmetry and symmetric constellations of features.” *Proc. of the 9th European Conference on Computer Vision*, 2:508-521.
- [16] Prasad, V.S.N., Davis, L.S. (2005). “Detecting rotational symmetries.” *Proc. of the Tenth IEEE International Conference on Computer Vision*, 2:954-961.
- [17] Haralick, M., Shanmugam, K., Dinstein, I. (1973). “Texture features for image classification.” *IEEE Transactions on Systems, Man, and Cybernetics*. 3(6): 610.
- [18] Viola, P., Wells, W.M. (1997). “Alignment by maximization of mutual information.” *Int. J. Comput. Vis.* 24(2), 137–154.
- [19] Turner, M.R. (1986). “Texture discrimination by Gabor functions.” *Biol Cybern*. 55(2-3):71-82.
- [20] Doyle, S, Hwang, M, Shah, K, Madabhushi, A, Tomasezwski, J, Feldman, M. (2007). “Automated grading of prostate cancer using architectural and textural image features.” *Proc. of the International Symposium on Biomedical Imaging (ISBI)*, pp. 1284-87.
- [21] Field, D.J. (1987) “Relations between the statistics of natural images and the response properties of cortical cells.” *J. Opt. Soc. Am. A*. 4(12):2379.
- [22] Koveti, P. (1995). “Image features from phase congruency.” Technical Report 95/4, University of Western Australia, Robotics and Vision Group.
- [23] Breiman, L., Friedman, J., Stone, C.J., Olshen, R.A. *Classification and Regression Trees*. Belmont: Wadsworth International Group; 1984.